Total-Body Low-Dose CT Image Denoising using Prior Knowledge Transfer Technique with Contrastive Regularization Mechanism

Minghan Fu, Yanhua Duan, Zhaoping Cheng, Wenjian Qin, Ying Wang, Dong Liang, *Senior Member, IEEE*, Zhanli Hu, *Senior Member, IEEE*

***Abstract*—Reducing the radiation exposure for patients in Total-body CT scan has attracted extensive attention in the medical imaging community. Given the fact that low radiation dose may result in increased noise and artifacts, which greatly affected the clinical diagnosis. To obtain high-quality Total-body Low-dose CT (LDCT) images, previous deep-learning based research work has introduced various network architectures. However, most of these methods only adopt Normal-dose CT (NDCT) images as ground truths to guide the training of the denoising network. Such simple restriction leads the model to less effectiveness and makes the reconstructed images suffer from over-smoothing effects. In this paper, we propose a novel intra-task knowledge transfer method that leverages the distilled knowledge from NDCT images to assist the training process on LDCT images. The derived architecture is referred to as the Teacher-Student Consistency Network (TSC-Net), which consists of the teacher network and the student network with identical architecture. Through the supervision between intermediate features, the student network is encouraged to imitate the teacher network and gain abundant texture details. Moreover, to further exploit the information contained in CT scans, contrastive regularization mechanism (CRM) built upon contrastive learning is introduced. CRM performs to pull the restored CT images closer to the NDCT samples and push far away from the LDCT samples in the latent space. In addition, based on the attention and deformable convolution mechanism, we design a Dynamic Enhancement Module (DEM) to improve the network's transformation capability. Extensive experimental results and clinical readings have demonstrated that the TSC-Net outperforms the state-of-the-art methods in both quantitative and qualitative evaluations.**

***Index Terms*—Knowledge transfer, Contrastive learning, Total-body CT reconstruction, Low-dose CT denoising.**

This work was supported by the National Natural Science Foundation of China (32022042, 81871441), the Shenzhen Excellent Technological Innovation Talent Training Project of China (RCJC20200714114436080), the Natural Science Foundation of Guangdong Province in China (2020A1515010733), Chinese Academy of Sciences Key Laboratory of Health Informatics in China (2011DP173015).

Corresponding author: Zhanli Hu, e-mail: zl.hu@siat.ac.cn

Minghan Fu, Yanhua Duan, Zhaoping Cheng as the co-first author.

Minghan Fu, Wenjian Qin, Dong Liang, Zhanli Hu are with the Lauterbur Research Center for Biomedical Imaging, Shenzhen Institute of Advanced Technology, Chinese Academy of Sciences, Shenzhen 518055, China and also with the Chinese Academy of Sciences Key Laboratory of Health Informatics, Shenzhen 518055, China.

Yanhua Duan and Zhaoping Cheng are with Department of PET/CT, The First Affiliated Hospital of Shandong First Medical University, Shandong Provincial Qianfoshan Hospital, Jinan 250014, China.

Ying Wang is with the Central Research Institute, United Imaging Healthcare Group, Shanghai 201807, China.

I. Introduction

X-RAY Computed Tomography (CT) is a widely used medical imaging modality for clinical diagnosis. Nevertheless, its high radiation dose, especially in Total-body CT scan cases, poses a serious concern. The enormous radiation received by patients will increase the potential risk of getting diseases, such as leukemia [1] and cancer [2]. To avoid the harm of high-level dose CT scan, decrease the tube-current-time [3] or tube-voltage [4], [5] techniques have been studied and widely used in the past few decades. As a result, the signal-to-noise ratio (SNR) collected from low-dose CT (LDCT) images is much lower than that of normal-dose CT (NDCT) scans. Higher photon statistical noise in LDCT images impedes clinical diagnostic. Thus, improving the image quality of LDCT scans has attracted extensive attention in the medical image processing community. Many noticeable research works have been proposed, which can be roughly divided into four categories: 1) sinogram domain filtering, 2) iterative reconstruction (IR), 3) traditional-based image processing methods and 4) deep learning (DL) based postprocessing methods.

Sinogram domain filtering methods is to process the 2D sinogram signals before image reconstruction. Based on this idea, a series of works have been proposed , such as penalized weighted least-squares (PWLS) [6], [7], bilateral filtering [8], and structural adaptive filtering methods [9], [10] . However, LDCT scans reconstructed by the above algorithms tend to lose structure information and spatial resolution in the image domain, for instance, edges and favorable texture details.

Iterative reconstruction (IR) algorithms take the scanner geometry and physical properties into consideration. Total variation [11] and its variants [12], [13] are representatives of the IR-based methods. They formulate that the signal is piecewise constant, this strong assumption causes the undesired side effect. In addition, due to the iterative nature, IR-based methods require unacceptable computational costs.

Some traditional-based image processing methods are also fit to LDCT denoising, such as the non-local means (NLM) [14] and the block-matching 3D (BM3D) algorithm [15]. BM3D algorithm grouped similar 2D CT image patches into 3D arrays, by applying 3D transform and corresponding coefficients filtering to achieve better results. Although it can improve the image quality effectively, residual errors are still exists due to the non-uniformly distributed noise in CT images.

With the rising up of deep learning techniques, many convolutional neural networks (CNN) have been widely conducted in solving LDCT image reconstruction and achieved a significant breakthrough. [16] is the pioneering work that designs a noise reduction method by training a convolutional neural network (CNN) patch-by-patch. They continue to improve this original work by integrating auto-encoder structure, transposed convolution layers and residual blocks into a residual encoder-decoder neural network, namely RED-CNN [17]. Chen et al. [18] propose a learned expert assessment-based reconstruction network, namely LEARN. Request on the LDCT data-driven and iterative scheme, the 'LEARN' can estimate the key parameters accurately and suppress most of the noise. Reference [19] suggests a PDF network that uses multilayer perceptrons (MLPs) to process different geometries and dose information. The outputs of the MLPs are used as additional knowledge to aid LDCT image reconstruction. Limited CT dataset will impede the model performance, towards this issue, [20] extracts overlapped patches from LDCT images to form patch manifolds. By optimizing parameters in both image and manifold spaces, the network achieves excellent denoising performance. Considering the over-smooth effect of network reconstructed CT images, generative adversarial training [21] as well as the perceptual loss [22] are integrated. Wolterink et al. [23] introduce a conditional GAN (CGAN) [24] structure into LDCT image denoising. The generator not only trains to minimize the distance between reconstructed LDCT images and NDCT counterparts but also needs to generate high-quality outputs to cheat the discriminator, which enables the model to avoid blur artifacts. Yang et al. [25] utilize Wasserstein distance instead of JS divergence [26] to measure the differences between distributions of generated fake images and real images. They also use a pre-trained VGG-19 network [27] to extract image features and minimize the distance in representation space as additional supervision. Based on the cycle consistency structure [28], Dong et al. propose a cycle-consistent deep attention network [29] for multiorgan segmentation. Liu et al. develop a CycleGAN-based method [30] for cone-beam CT (CBCT) image enhancement.

However, most of these existing methods use normal-dose CT information insufficiently. In particular, they simply adopt NDCT images as ground truths to guide the training of the denoising network via L1/L2 based image reconstruction loss or introduce adversarial loss to auxiliary training. But only using such constraints can not effectively recover the favorable details in LDCT images. They ignore the fact that the low-dose CT images and normal-dose corresponding scans contain the same visual content.

Could we make much greater use of NDCT scans? Inspired by knowledge distillation [31], [32] and hint-based learning [33], which migrates the information from the teacher network to the student network. We propose a two-stage knowledge transfer method that utilizes NDCT images to train for a teacher network in the first stage. The well-trained teacher network contains abundant and robust prior knowledge in the CT image domain. In the second stage, we minimize the intermediate features of the teacher and student network for encouraging the denoising student network to imitate the teacher network as well as achieve the knowledge transfer purpose. Moreover, to further exploit the information in LDCT and NDCT images, we introduce a contrastive regularization mechanism (CRM). LDCT images, reconstructed images and NDCT images are treated as negative samples, anchor samples and positive samples, respectively. CRM aims to pull the anchor points closer to the positive points and pushes away that from the negative points in the latent space. In other words, CRM minimizes the L2 distance from the prediction results to the upper bond and maximizes that between the lower bond and the prediction results. In addition, the Dynamic Enhancement Modules are adopted, which can dynamically expand the receptive field for fusing more spatially structured information. By integrating the above novel mechanisms, the performance of our proposed TSC-Net gets remarkable improvement.

To sum up, the main innovations is on four aspects:

(1) We explore the Total-body low-dose CT image reconstruction problem. Instead of designing multiple networks for the different anatomical site processing tasks, our proposed TSC-Net can directly restore LDCT images from each anatomical site and achieve pleasant results for clinical diagnosis.

(2) Inspired by knowledge distillation [31], [32], which migrates knowledge from the teacher network to the student network. We propose a knowledge transfer method that utilizes identical NDCT image pairs to train for a teacher network. The trained teacher network can provide robust prior information to aid the training of the student network, which leads the student network to reconstruct high-quality CT images.

(3) We introduce a contrastive regularization mechanism (CRM) to exploit both the information of low-dose Total-body CT scans and normal-dose counterparts. CRM guarantees that the restored LDCT scans are pulled closer to the NDCT scans and pushed far away from the LDCT scans in the representation space.

(4) Considering that the fixed geometric structures of convolution layers will impede the image and feature geometric transformations, we design a Dynamic Enhancement Module (DEM) that combines the channel attention [34] and deformable convolution modules [35], [36]. DEM not only lets the TSC-Net pay more attention to the important feature maps but also be more sensitive to spatially structured information.

II. RELATED WORKS

A. Knowledge Distillation

Knowledge distillation reduces the complexity of large, cumbersome models (teacher networks) into smaller, faster models (student networks) and preserves model generalization ability in the meantime. [31] firstly introduces the idea of knowledge distillation. [37] and [38] explore distillation for transferring information between high-quality and low-quality image domains, which also indicate that knowledge distillation is not only useful for network compression but also can be applied in various computer vision tasks. Romero et al. [33] introduce a two-stage strategy for network training. According to their methodology, the teacher network middle layer provides 'hints' to guide the training of the student model.

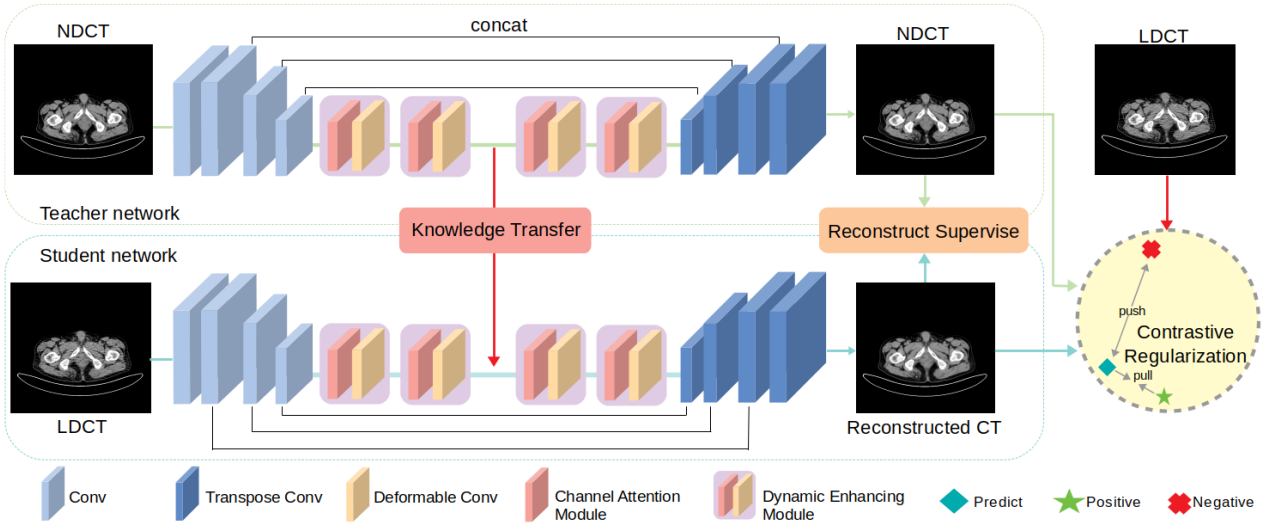

Fig. 1: The architecture of the proposed TSC-Net. It consists of the Teacher net and the Student net. They have identity network architecture. We jointly minimize the L1 and SSIM based reconstruction loss, knowledge transfer based feature-level loss and constructive regularization that pulls the restored image (i.e. anchor) close to the NDCT (i.e. positive) image and away from the LDCT image (i.e. negative).

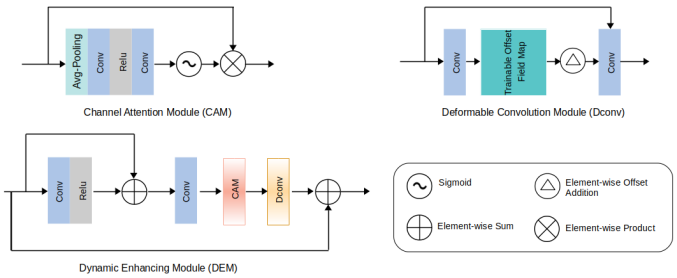

Fig. 2: Illustration of the Dynamic Enhancement Module (DEM).

Different from [37] and [33], where knowledge transfer is carried out among heterogeneous tasks, we perform Teacher-Student Consistency Network (TSC-Net) with the teacher and student both working on the CT image reconstruction task but taking NDCT data and LDCT data as their respective inputs.

B. Contrastive Learning

Dating back to Hadsell et al. [39], contrastive learning approaches learn representations by contrasting positive pairs against negative pairs. It is widely used in self-supervised representation learning [40]–[44]. For a model predicted anchor tensor, contrastive learning aims to pull the anchor close to positive points and push far away from negative points in the latent space. Previous works [43]–[45] often apply contrastive learning into high-level vision tasks, since these tasks are naturally suitable for establishing contrasts between positive and negative samples. Recently, the work in [46] and [47] demonstrate that the utilization of contrastive learning in low-level image processing tasks gains successful effects. Precisely, [46] proves its powerful performance on image-to-image translation case. [47] shows its potential in the image dehazing. We take the lead in introducing the contrastive regularization mechanism (CRM) into LDCT scan reconstucion task.

III. METHODOLOGY

In this section, we first outline the network architecture of the proposed Teacher-Student Consistency Network (TSC-Net). Then, the details and the sense of design for each key component are illustrated precisely. In the end, the loss functions adopted in training process are introduced.

A. Knowledge Transfer Technique

We propose a dual network, which contains a teacher network and a student network as shown in Fig. 1. Our Teacher-Student Consistency (TSC) structure refers to leveraging the knowledge acquired from NDCT images to facilitate the learning process of the same task on LDCT images. Specifically, the teacher network is trained by identical NDCT image pairs. During the training process, the teacher network gradually learns to restore NDCT images precisely. Accurate data distributions and semantic information in NDCT scans are gained. We use this well-trained teacher network to guide the training of the student network. In other words, we aim to let the teacher network learn the structural information from NDCT images in advance, and transfer such vital information as prior knowledge to the student network for high-quality LDCT image reconstruction.

Based on the U-Net [48] structure, we design an encoder-decoder architecture. The encoder consists of several convolution layers and the designed Dynamic Enhancement Modules (DEMs). The convolution layers are used for extracting feature maps and $4\times$ downsampled the input CT images. As shown in Fig. 2, the Dynamic Enhancement Module consists of channel attention module [34] and deformable convolution module [35], which aims to provide additional flexibility for the neural network in dealing with noisy regions. More structure details and interpretation of DEMs can be seen in Section III.C. The outputs of the encoder are deep and semantic features, we transfer the knowledge contained in the teacher network to the student network by minimizing the L1 distance of these crucial

feature maps. In this way, we increase the feature similarity between the middle layers so that the student network is encouraged to imitate the teacher network and gains abundant prior knowledge. In the decoder part, we use transposed convolution [49] operation to upsample the feature maps and let feature maps gradually recover to their original size as output. In addition, to preserve more detailed information and avoid gradient vanishing [50], multiple skip connections are added between encoder and decoder.

B. Contrastive Regularization Mechanism

To further dig as well as capture information from LDCT and NDCT image pairs that can be maximally used for anchor points prediction, we introduce a Contrastive Regularization Mechanism (CRM). To achieve that, two aspects need to be clarified. One is to select the positive samples and negative samples, the other is to find a proper metric space for these sample pairs and prediction results to perform contrast calculations. Towards these two targets, we use the following strategies. First, we define the network reconstructed CT images as anchor samples, LDCT images as negative samples, and NDCT images as positive samples, as shown in Fig. 1. Also, we can treat the NDCT images as the upper bound and LDCT images as the lower bound for computing. Then we extract the feature maps for all the samples and anchors from shallow layers to deep semantic layers by a fixed pre-trained VGG-16 Network [27] to form the latent metric space. By minimizing the L2 distance from anchor points to positive points, and maximizing that from anchor points to negative points, the predicted CT images are pushed closer to NDCT images and apart far away from the LDCT images. Experiments demonstrate our CRM enhances denoised CT image quality to a large extend, discussions and results are shown in Section IV.B.

C. Dynamic Enhancement Module

The architecture of designed dynamic enhancement module is shown in Fig. 2. DEM is composed of channel attention block [34] and deformable convolution block [35], [36]. The channel attention block is learned to give different weights to each channel of the input feature maps. The important channel will get higher considerations and feed a larger value that is computed by the sigmoid function [51]. Moreover, in view of the drawback of fixed grid kernel as shown in Fig. 3 middle, which limits the receptive field and cannot exploit the structured information in the feature space [52]. We introduce deformable convolution to replace part of the normal convolution operations to form the designed DEM. As shown in Fig. 3 right, the deformable convolution is more sensitive to the edge information since the kernel is dynamic and flexible, which greatly raises the model transformation capability for better CT image reconstruction. By placing DEMs between the encoder and decoder, the network can dynamically give more attention to the computation of the interest regions and fuse more spatially structured information.

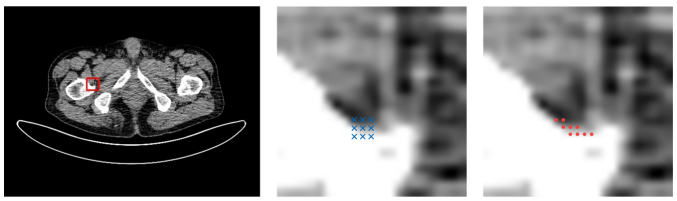

Fig. 3: Visualization of the difference between normal grid convolution kernel (middle) and deformable convolution kernel (right) on processing an input LDCT image (light).

D. Objective Functions

We denote our reconstructed image as I^{rec}. I^{nd} and I^{ld} stand for NDCT images and LDCT images. The teacher network, student network and the VGG-16 [27] pre-trained on ImageNet [53] network are represented as T, S and E respectively.

Fidelity Loss. The commonly used fidelity losses include MSE and L1. As MSE loss is relatively high sensitive to outliers, thus always suffer from gradient explosion [54]. Although the L1 loss does not have this issue, it cannot be differentiable at zero. The smooth L1 loss is a combination of the above two losses, benefiting from their merits and avoiding their drawbacks. We use it as our fidelity loss to quantitatively measure the difference between I^{rec} and I^{nd}.

$I_c^{rec}(i)$ and $I_c^{nd}(i)$ denote the intensity of the c-th channel of pixel i in the reconstructed images and in the NDCT images respectively, and N denotes the total number of pixels in each channel. The Fidelity Loss can be defined as:

$$\mathcal{L}_{\mathrm{F}} = \frac{1}{3N}\sum_{i=1}^{N}\sum_{c=1}^{3}\alpha\left(I_c^{rec}(i) - I_c^{nd}(i)\right) \tag{1}$$

where

$$\alpha(e) = \begin{cases} 0.5e^2, \text{ if } |e| < 1 \\ |e| - 0.5, \text{ otherwise} \end{cases} \tag{2}$$

Multi-Scale SSIM Loss. Let O and G denote two windows of common size centered at pixel i in the reconstructed image and the NDCT image, respectively. Use a Gaussian filter to O and G, and compute the resulting means μ_O, μ_G, standard deviations σ_O, σ_{G_1} and covariance σ_{OG}. The SSIM for pixel i is defined as:

$$\begin{aligned} \mathrm{SSIM}(i) &= \frac{2\mu_O\mu_C + C_1}{\mu_O^2 + \mu_G^2 + C_1} \cdot \frac{2\sigma_{OG} + C_2}{\sigma_O^2 + \sigma_G^2 + C_2} \\ &= l(i) \cdot \mathrm{cs}(i) \end{aligned} \tag{3}$$

where $l(i)$ represents luminance and $cs(i)$ represents contract and structure measures, C_1, C_2 are two variables to stabilize the division with weak denominator. The MS-SSIM loss is computed using M levels of SSIM. We have:

$$\mathcal{L}_{\text{MS-SSIM}} = 1 - \text{MS-SSIM} \tag{4}$$

where

$$\text{MS-SSIM} = l_M^{\alpha}(i) \cdot \prod_{m=1}^{M} cs_m^{\beta_m}(i) \tag{5}$$

with α and β_m being default parameters.

Knowledge Transfer Loss. The teacher network aims to learn the structure information from the NDCT images as prior knowledge and transfer it to the student network. To achieve our purpose, Knowledge Transfer Loss is adopted, which guides the features from the student network to mimic the ones from the teacher network by reducing their L1 distance. We denote the median feature maps by F_{mid} and use the superscript T and S to indicate whether they come from the teacher or student network. Specifically, F_{mid}^{T} denotes the feature maps of the second DEM's output of the teacher network, F_{mid}^{S} denotes the feature maps of the second DEM's output of the student network. Our Knowledge Transfer Loss can be formulated as:

$$L_{KT} = \left\| F_{mid}^{S} - F_{mid}^{T} \right\|_1 \tag{6}$$

Contrastive Regularization. To pull reconstructed images (anchor samples) close to NDCT images (positive samples) and push away from LDCT images (negative samples). Instead of directly doing the minimization calculation on the pixel level, we use a fixed VGG-16 network to extract multi-layer features as predicted, positive and negative samples to form the metric space. We conduct the following regularization term:

$$\mathcal{L}_{\mathrm{C}} = \sum_{i=1}^{N} \beta_i \cdot \frac{1}{C_l H_l W_l} \cdot \frac{\| E_i\left(I^{nd}\right) - E_i\left(I^{rec}\right)\|_2^2}{\| E_i\left(I^{ld}\right) - E_i\left(I^{rec}\right)\|_2^2} \tag{7}$$

where E_i , i = 1, 2, 3 extracts the i-th hidden features from the pre-trained VGG-16 network last layer of each of the first three stages (i.e., Conv1-2, Conv2-2 and Conv3-3). We use the L2 distance loss after each extracted representations and set their corresponding weight coefficients $\beta_i, i = 1, 2, 3$ to $\frac{1}{4}, \frac{1}{2}, 1$, respectively. C_l, H_l, and W_l specify the dimension of output feature maps.

Total Loss. We combine the Fidelity Loss, MS-SSIM Loss, Knowledge Transfer Loss and Contrastive Regularization together to supervise the training of our TSC-Net.

$$\mathcal{L}_{total} = \mathcal{L}_{\mathrm{F}} + \mathcal{L}_{KT} + \alpha \mathcal{L}_{\text{MS-SSIM}} + \beta \mathcal{L}_{c} \tag{8}$$

where $\alpha = 0.1, \beta = 0.001$ are the hyperparameters weighting for each loss functions.

IV. EXPERIMENTS

In this section, we perform experiments to validate the effectiveness of the proposed method. First, the clinical dataset, training details and evaluation metrics are introduced. Second, we conduct ablation studies to illustrate useful insights into the loss functions and constituent modules of the TSC-Net. Finally, we evaluate the performance of the proposed TSC-Net with two representatives traditional-based methods (TV [11] and BM3D [15]) and four advanced deep-learning based methods (CNN [16], RED-CNN [17], WGAN-VGG [25] and Cycle-GAN [23]).

TABLE I: SCANNING PARAMETER SETTINGS FOR TOTAL-BODY CT IMAGES UNDER A uEXPLORER PET/CT SCANNER

Parameters	LDCT	NDCT
Source-to-detector distance (mm)	800	800
Source-to-patient distance (mm)	$300 \sim 500$	$300 \sim 500$
Tube voltage (kVp)	120	120
Tube Current (mA)	$200 \sim 500$	10
Thickness (mm)	3.0	3.0
Reconstruction Matrix	512×512	512×512

A. Experiment Setup

1) Clinical Patient Data Acquisition: With the clinical data supported by the first affiliated hospital of Shandong First Medical University (Jinan, Shandong, China), we utilize Total-body CT image pairs collected from 100 patients between September 2020 and March 2021 as our training and testing dataset. The age distribution for these patients ranges from 14 to 81. Among these patients, 54 of them are male and the other 46 patients are female. The total number of CT images is nearly 30 000 slices. The dataset contains high-resolution total-body normal-dose CT images for clinical diagnosis and their corresponding low-dose CT images for attenuation correction (AC). 90% of the data are used as training data and the other 10% of the data are used as testing data. These research CT image pairs are acquired under a uEXPLORER Total-body PET/CT scanner (Produced by United Imaging Healthcare Group, Shanghai, China). As shown in Table I, for the clinical normal-dose CT images, the scan tube voltage is 120 kVp and the thickness is 3 mm. According to different situations of patients, the scan tube current is set to different values by using the dose modulation technology. For the LDCT images, the scan tube current is uniformly set to 10 mAs and other settings are as same as that in NDCT scans.

2) Implementation Details: We implement our model in the PyTorch 1.9.1 framework on Ubuntu 18.04 with an NVIDIA RTX 3090 GPU during the training and testing process. While the raw CT images in the training dataset have a resolution of 512×512 pixels, we randomly rotate each image by 90,180,270 degrees and conduct horizontal flips as our data augmentation strategies. During the first training stage, we set the batch size to 4. Adam optimizer (β_1=0.9,β_2=0.999) is used for gradient descent. In addition, we conduct a specific decay strategy, where the initial learning rate is set to 1e-4 and decays 0.5 times at the 2nd, 4th epoch for a total of 10 epochs. Then we fix the parameters in the well-trained teacher network and use mid-feature maps as feature-level ground truths to auxiliary the second stage training. Different from teacher network training, for the whole TSC-Net training, we set the batch size to 2 due to the limited GPU memory size. Knowledge Transfer Loss and Contrastive Regularization are introduced as extra supervision. The start learning rate is set to 1e-4 and decays 0.5 times at the 10th, 20th epoch for a total of 35 epochs. Other training settings are the same as those in the first training stage.

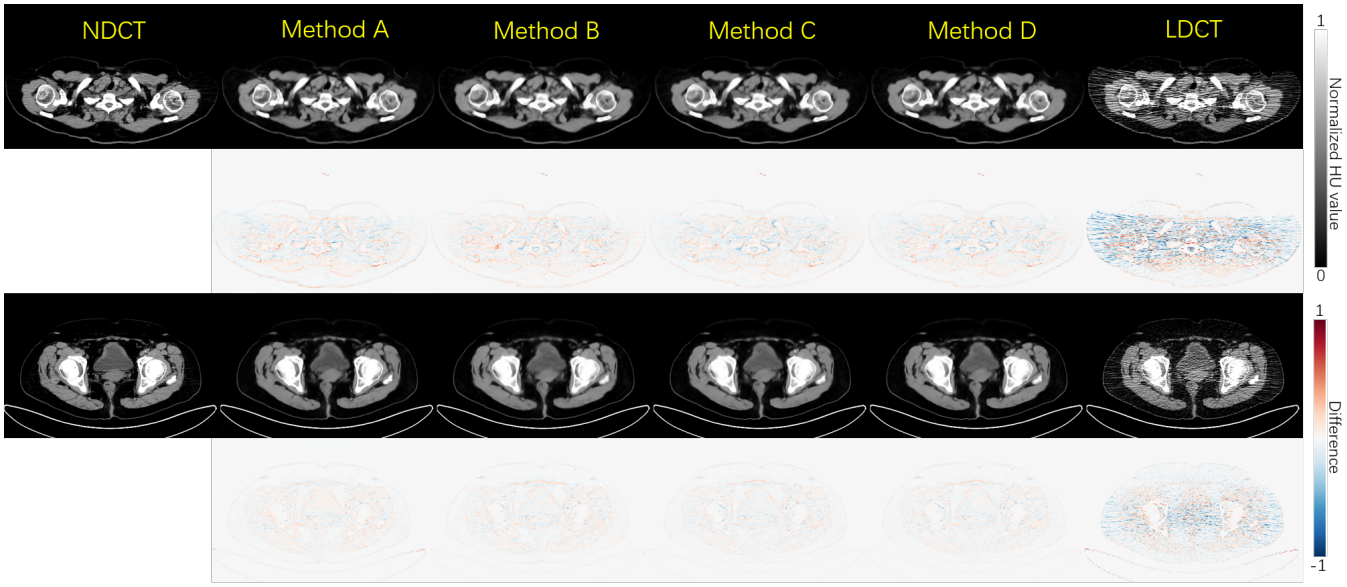

Fig. 4: Quantitative comparisons of different LDCT reconstruction methods. Method A is the baseline of our model, Method B adds four DEMs on the baseline, Method C further introduces the Knowledge Transfer Loss to auxiliary network training, and Method D is the proposed TSC-Net. The display-window is set to [40 HU, 400 HU].

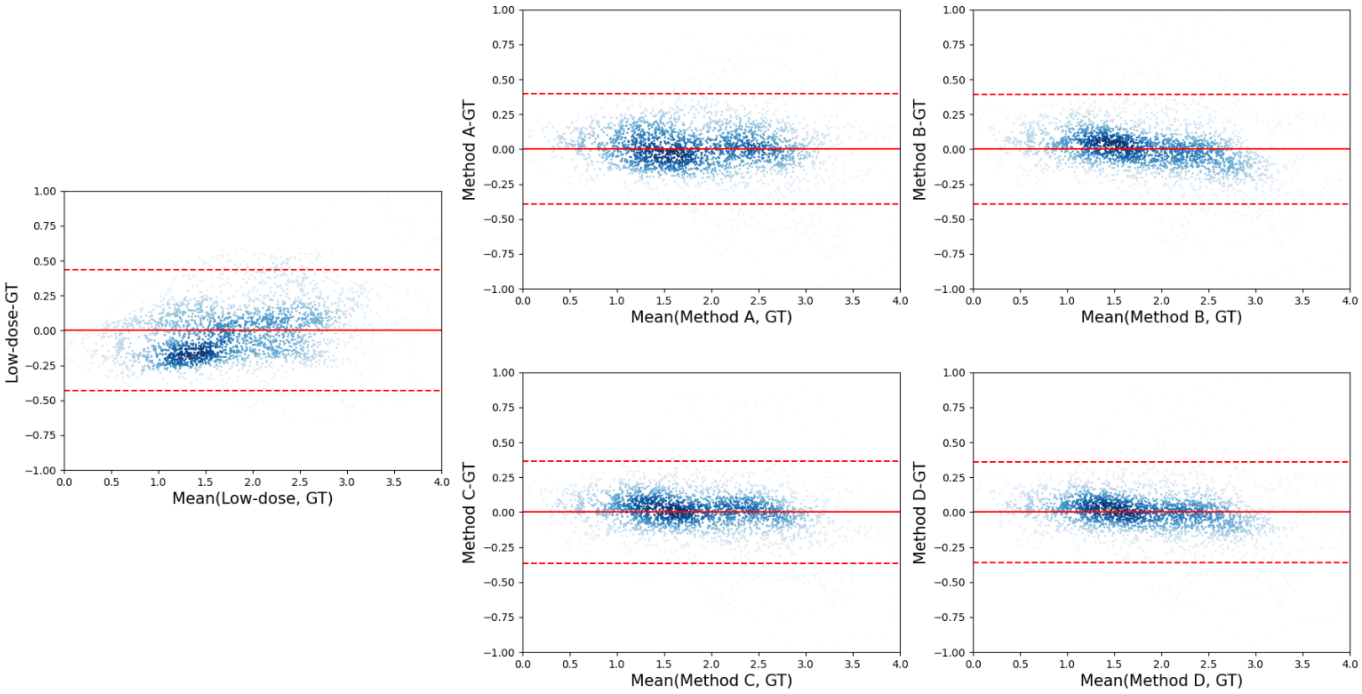

Fig. 5: Bland-Altman 2-D histograms of PSNR value compared between methods (Ground-truth to low-dose CT images and method A, B, C, and D) across all the clinical test data. The solid and dashed lines denote the mean and 95% confidence interval of the PSNR differences respectively. The color represents relative frequency in a range of 0 to 10. The brighter color indicates high density.

3) Evaluation Metric: We use three computational metrics to evaluate the performance of our networks, including peak signal-to-noise ratio (PSNR), the structural similarity index (SSIM) [55], and the root mean square error (RMSE). To judge clinical performance, two expert radiologists scored image quality on a 5-point scale (1 = uninterpretable,2 = poor, 3 = adequate, 4 = good, 5 = excellent). Scores are dichotomized into 1–3 vs. 4–5 to analyze the percentage of images with high scores. Kappa statistics [56] are applied as the consistency test.

B. Ablation Study of Proposed Methods

To demonstrate the effectiveness of our TSC-Net, we perform the ablation studies to analyze different elements, including DEM (dynamic enhancement module), KT (knowledge transfer) and CRM (contrastive regularization mechanism).

We first construct our base network as the baseline of the LDCT image denoising network, which mainly consists of several convolutional downsampling layers and Transpose-

TABLE II: Quantitative results (mean±sd of PSNR, SSIM and RMSE) associated with the base model as well as method A, B, C, and D for the images in the clinical testing dataset. The best results are in bold.

Methods	PSNR (mean ± std) ↑	SSIM (mean ± std) ↑	RMSE (mean ± std) ↓
Low-dose CT	21.40 ± 2.59	0.8182 ± 0.0550	0.3840 ± 0.0992
Baseline (Method A)	26.06 ± 2.57	0.8736 ± 0.0416	0.2255 ± 0.0627
Baseline+DEM (Method B)	26.13 ± 2.54	0.8751 ± 0.0408	0.2237 ± 0.0619
Baseline+ DEM + KT (Method C)	26.20 ± 2.56	0.8788 ± 0.0402	0.2218 ± 0.0618
Baseline+ DEM + KT+ CRM (Method D)	**26.23 ± 2.57**	**0.8811 ± 0.0388**	**0.2212 ± 0.0614**

TABLE III: Quantitative results (mean±sd of PSNR, SSIM and RMSE) associated with different algorithms for the images in the clinical testing dataset. The best results are in red and the second ranked results are in blue.

	PSNR ↑		SSIM ↑		RMSE ↓	
Methods	mean ± std	p-value	mean ± std	p-value	mean ± std	p-value
LDCT	21.40 ± 2.59	–	0.8182 ± 0.0550	–	0.3840 ± 0.0992	–
TV	22.67 ± 2.55	$2.17e^{-5}$	0.8258 ± 0.0538	0.0008	0.3318 ± 0.0861	$3.86e^{-6}$
BM3D	22.91 ± 2.26	$0.22e^{-3}$	0.8192 ± 0.0495	0.5395	0.3211 ± 0.0773	$3.86e^{-5}$
CNN	25.62 ± 2.47	$3.68e^{-12}$	0.8672 ± 0.0405	$1.92e^{-5}$	0.2367 ± 0.0645	$7.33e^{-17}$
RED-CNN	26.08 ± 2.57	$1.36e^{-14}$	0.8778 ± 0.0398	$1.143e^{-8}$	0.2251 ± 0.0634	$4.87e^{-17}$
WGAN-VGG	25.69 ± 2.51	$2.88e^{-12}$	0.8706 ± 0.0401	$6.32e^{-6}$	0.2351 ± 0.0652	$8.24e^{-17}$
Cycle-GAN	26.08 ± 2.52	$7.08e^{-15}$	0.8684 ± 0.0424	$1.80e^{-7}$	0.2250 ± 0.0621	$4.59e^{-17}$
TSC-Net	26.23 ± 2.57	$3.64e^{-11}$	0.8811 ± 0.0388	$1.49e^{-9}$	0.2212 ± 0.0614	$3.28e^{-15}$

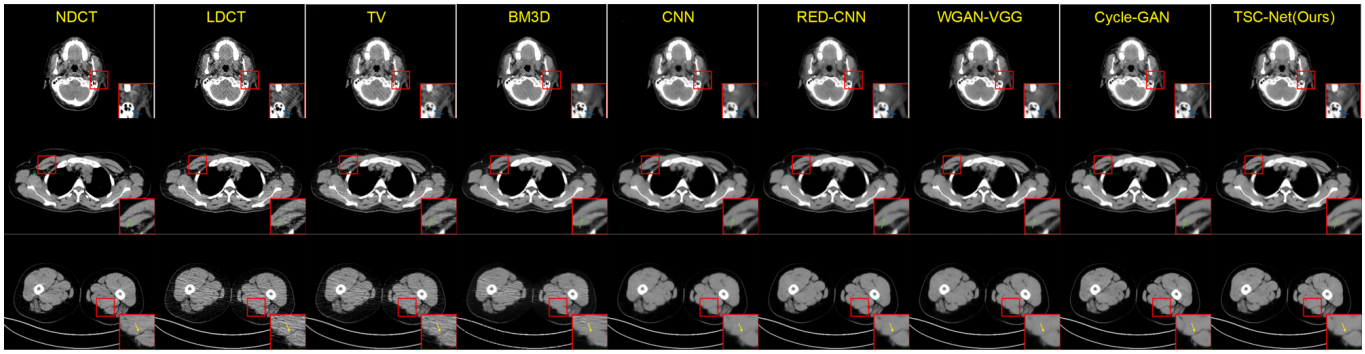

Fig. 6: Quantitative comparisons of the proposed methods with other methods. ROIs are marked by red rectangles. Zoomed ROI images are placed in the bottom right corner. The arrows indicate regions containing features revealed differently by the competing algorithms.

convolution upsampling layers in symmetry. Moreover, inspired by residual learning, multiple skip connections are introduced to facilitate the training process.

Subsequently, we add the different modules into the base network as (1) **Baseline+DEM**: Add the four dynamic enhancing modules into baseline, which are followed by the 4× downsampling layer. (2) **Baseline+DEM+KT**: Add four DEMs and introduce the well-trained teacher network to provide feature-level supervision as knowledge transfer loss during the student network training process. (3) **Proposed method**: The combination of our student network, knowledge transfer techniques and the proposed contrastive regularization mechanism that allows both negative and positive samples to auxiliary model training.

We employ Fidelity loss (Eq.1) and Multi-Scale SSIM loss (Eq. 5) as image reconstruction loss. The performance of these models is summarized in Table II. We use the clinical dataset provided by the first affiliated hospital of Shandong First Medical University as the training set and testing set.

DEM improves the performance from baseline to baseline+DEM with an increase of 0.07dB PSNR. Therefore, DEM is an important factor due to the higher performance gains. We also evaluate the number of DEMs and set the number of Dynamic Enhancement Modules to 2, 4, and 6. The quantitative results would improve as the network depth increases, we notice that there is no more significant improvement when the number increase to 6. Thus, we set the number of DEMs to 4, which makes a great trade-off between computation cost and model efficiency. Moreover, the knowledge transfer techniques significantly improve the performance on PSNR, SSIM and RMSE with the gains of 0.07dB increase,0.0037 increase and 0.0019 decrease, respectively. Since the knowledge transfer loss makes the student network imitates the teacher network to reconstruct normal-dose CT images. It is a fact that the prior knowledge provided by the teacher network is quite useful in enhancing the denoising performance of the student

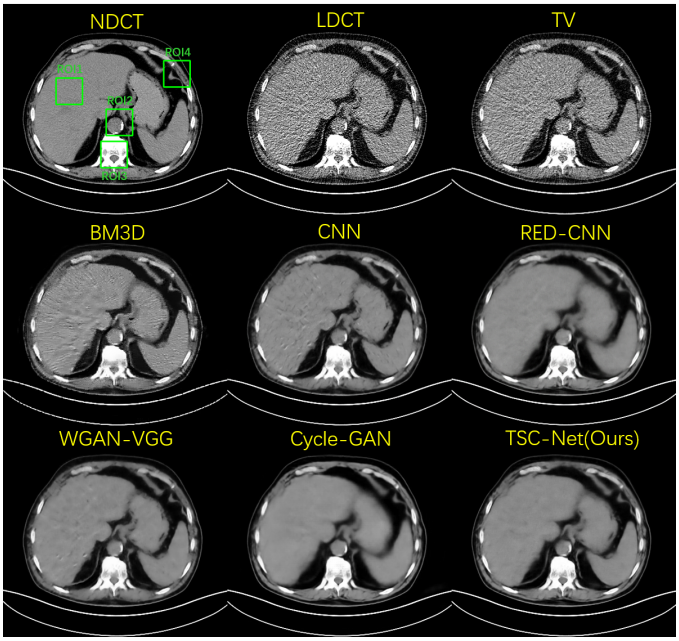

Fig. 7: Prediction results companion between different methods. The green boxes indicate the four ROIs.

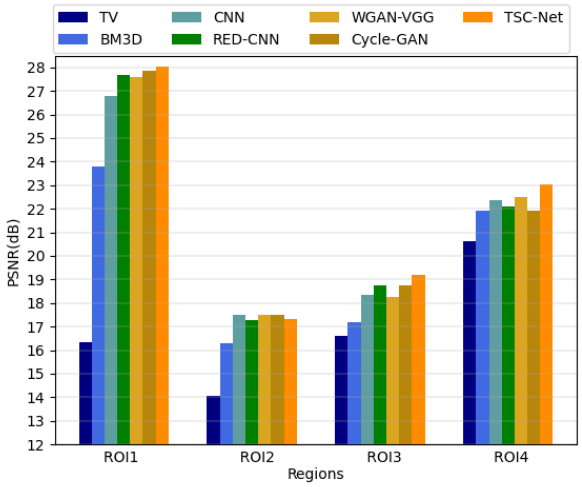

Fig. 8: Statistical results for the differnet ROIs marked in Fig. 7.

network. Our TSC-Net also employs the CRM to further utilize both negative and positive samples for training. By adding the proposed CRM, TSC-Net achieves the best performance on the clinical test dataset.

Fig. 4 illustrates the visual effect and the differences between images processed by different methods, where it can be observed more clearly that the proposed TSC-Net adding knowledge transfer loss and contrastive regularization (Method D) generates the smallest difference and achieves the best restored results, proving that it can preserve the majority of details and suppress most noise and artifacts. In Fig. 5, the statistics results show that Method C and Method D have a more constricted distribution towards the red center line, indicating a better correlation to normal-dose CT images.

C. Denoising Result Comparison

1) Qualitative Visual Effect Comparison: We show the visual quality comparisons in Fig. 6. Three representative CT slices from the testing set are used to demonstrate the performance of our proposed method and we placed the zoomed 150×150 region-of-interest (ROI) marked by the red rectangle on the bottom right corner of each scan. All these methods demonstrate capabilities to remove the noise from the LDCT image to different extents. However, TV [11] and BM3D [15] cannot eliminate the streaking artifacts efficiently. CNN [16] and RED-CNN [17] can remove most of the noise but suffer a lot from the over-smoothing problem. As shown by the blue arrows on the first row of Fig. 6, we can see more clearly that different mastoid air chambers are fuse together. It is mainly because they simply adopt the MSE as the loss of the network, making the network only focus on the pixel-wise difference elimination but overlook the perceptual effect preservation of the whole image structure. WGAN-VGG [25] and Cycle-GAN [28] have better improvement on preserving structures by introducing adversarial loss as extra supervision. However, the green and yellow arrows in Fig. 6 demonstrates that they are not sensitive to edge information and always tend to lose the favorable image details. Our proposed TSC-Net utilizes the Dynamic Enhancement Modules, Knowledge Transfer Techniques and Contrastive Regularization Mechanism, which further exploit the information contained in both NDCT and LDCT images. Most notably, the well-trained teacher network produces robust prior knowledge that makes the student network gain more image structure and detailed information for LDCT image restoration. TSC-Net achieves the best performance in balancing noise removal and structure preservation without introducing unnecessary artifacts.

2) Quantitative Results Comparison: The comparison results for different local ROIs are shown in Fig. 7, we selected four ROIs, which are marked with green boxes, including the liver, aorta, backbone and muscle tissues in the abdomen site. As shown in Fig. 8, the statistical results for the PSNR demonstrate that the TSC-Net outperforms other methods on most of the local regions and is only slightly lower than that in Cycle-GAN [28] on ROI3. To evaluate the denoising performance for different sites, we randomly select one patient's slices which consists of 230 CT scans from cranium to pelvis as testing data. The proposed TSC-Net has the best reconstruction results on nearly every site except a few slices. For the whole test dataset, the qualitative results are shown in Table III. The performance of our method surpasses the second-ranked competitors by a large margin in terms of all the metrics. In addition, the p-values prove that the higher PSNR, SSIM and lower RMSE values have statistical significance, which indicates that the proposed TSC-Net has excellent performance over all the clinical testing data.

3) Inference Time Comparison: We compare the inference time with these methods for processing one 512×512 image by an NVIDIA RTX3090 GPU. TV [11] and BM3D [15] take longer time to complete denoising process, which is 1.24s and 1.44s separately. For other deep-learning based methods, time consuming are nearly the same. CNN [16] method takes 0.077s

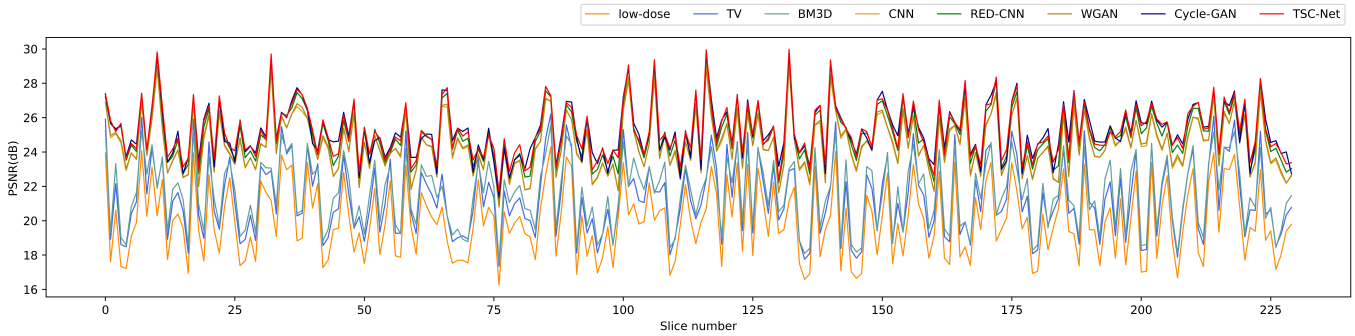

Fig. 9: Quantitative results comparison of different methods for one patient total-body (from cranium site to pelvis site) CT scans.

TABLE IV: Agreement between the readers and assigned quality score across different image types.

Metrics	LDCT	TSC-Net	NDCT
Average Quality Score	2.63 ± 0.70	4.02 ± 0.56	4.89 ± 0.36
High Score Percentage	6.2%	90.5%	98.87%
Kappa Coefficient	36.15%	52.98%	63.30%

for single LDCT image processing, WGAN-VGG [25] is followed by taking 0.079s. RED-CNN [17] and proposed TSC-Net take 0.0832s and 0.089s separately. Cycle-GAN [28] takes the longest processing time for 0.091s. It is a decisive fact that our approach has the best performance both qualitatively and quantitatively with similar processing time.

D. Clinical readings

As shown in Table IV, the average image quality scores and high-score percentage assigned by each reader prove the power of our proposed TSC-Net. By conducting TSC-Net on LDCT image enhancement, the ratio of high-quality scans raises from 6.2% to 90.5% and the average value increases by 1.39 compared with original LDCT images. For consistency analysis, the readers have much more agreement with each other on TSC-Net enhanced CT scans than that in LDCT images. It is not surprising to see that NDCT images achieve the best score on each metric since they use high-radiation exposure to achieve high-quality CT scans for clinical diagnosis.

V. Conclusion

In conclusion, we propose the TSC-Net with novel network architecture for Total-body low-dose CT image denoising. The designed dynamic feature enhancement module benefits from preserving information flow adaptively and enhances the denoising network transformation capability. To further exploit the favorable texture details and structure information in NDCT images, we utilize the knowledge transfer technique and contrastive regularization mechanism. Teacher-Student Consistency architecture leverages the knowledge distilled from NDCT image to assist the learning process on LDCT image denoising by supervising the intermediate feature maps during the training process. The similar data distribution of middle feature maps leads the student network to generate high-quality reconstructed images. The contrastive regularization mechanism is built upon contrastive learning to ensure that the restored image is pulled closer to the NDCT images and pushed far away from the LDCT image in representation space. We have comprehensively evaluated the performance of the proposed TSC-Net on a clinical dataset, which demonstrates the superior performance gains over all the other SOTA methods. Clinical readings also proved that our method significantly enhances the quality of Total-body low-dose CT images.

References

[1] Donald W Polhemus and Richard Koch. Leukemia and medical radiation. *Pediatrics*, 23(3):453–461, 1959.

[2] Zachary S Kelm, Daniel Blezek, Brian Bartholmai, and Bradley J Erickson. Optimizing non-local means for denoising low dose ct. In *2009 IEEE International Symposium on Biomedical Imaging: From Nano to Macro*, pages 662–665. IEEE, 2009.

[3] Yang Chen, Wufan Chen, Xindao Yin, Xianghua Ye, Xudong Bao, Limin Luo, Qianjing Feng, Xiaoe Yu, et al. Improving low-dose abdominal ct images by weighted intensity averaging over large-scale neighborhoods. *European Journal of Radiology*, 80(2):e42–e49, 2011.

[4] Yumi Yanaga, Kazuo Awai, Yoshinori Funama, Takeshi Nakaura, Toshinori Hirai, Sebastien Roux, and Yasuyuki Yamashita. Low-dose mdct urography: feasibility study of low-tube-voltage technique and adaptive noise reduction filter. *American Journal of Roentgenology*, 193(3):W220–W229, 2009.

[5] Adeel R Seyal, Atilla Arslanoglu, Samir F Abboud, Azize Sahin, Jeanne M Horowitz, and Vahid Yaghmai. Ct of the abdomen with reduced tube voltage in adults: a practical approach. *Radiographics*, 35(7):1922–1939, 2015.

[6] Shaojie Tang and Xiangyang Tang. Statistical ct noise reduction with multiscale decomposition and penalized weighted least squares in the projection domain. *Medical physics*, 39(9):5498–5512, 2012.

[7] Jing Wang, Tianfang Li, Hongbing Lu, and Zhengrong Liang. Penalized weighted least-squares approach to sinogram noise reduction and image reconstruction for low-dose x-ray computed tomography. *IEEE transactions on medical imaging*, 25(10):1272–1283, 2006.

[8] Armando Manduca, Lifeng Yu, Joshua D Trzasko, Natalia Khaylova, James M Kofler, Cynthia M McCollough, and Joel G Fletcher. Projection space denoising with bilateral filtering and ct noise modeling for dose reduction in ct. *Medical physics*, 36(11):4911–4919, 2009.

[9] Marc Kachelrieß, Oliver Watzke, and Willi A Kalender. Generalized multi-dimensional adaptive filtering for conventional and spiral single-slice, multi-slice, and cone-beam ct. *Medical physics*, 28(4):475–490, 2001.

[10] C-F Westin, J Richolt, V Moharir, and Ron Kikinis. Affine adaptive filtering of ct data. *Medical Image Analysis*, 4(2):161–177, 2000.

[11] Zhiqiang Chen, Xin Jin, Liang Li, and Ge Wang. A limited-angle ct reconstruction method based on anisotropic tv minimization. *Physics in Medicine & Biology*, 58(7):2119, 2013.

[12] Xiaoli Yang, Ralf Hofmann, Robin Dapp, Thomas Van de Kamp, Tomy dos Santos Rolo, Xianghui Xiao, Julian Moosmann, Jubin Kashef, and Rainer Stotzka. Tv-based conjugate gradient method and discrete l-curve for few-view ct reconstruction of x-ray in vivo data. *Optics express*, 23(5):5368–5387, 2015.

[13] Yi Liu, Hong Shangguan, Quan Zhang, Hongqing Zhu, Huazhong Shu, and Zhiguo Gui. Median prior constrained tv algorithm for sparse view low-dose ct reconstruction. *Computers in biology and medicine*, 60:117–131, 2015.

[14] Antoni Buades, Bartomeu Coll, and Jean-Michel Morel. Non-local means denoising. *Image Processing On Line*, 1:208–212, 2011.

[15] Aram Danielyan, Vladimir Katkovnik, and Karen Egiazarian. Bm3d frames and variational image deblurring. *IEEE Transactions on image processing*, 21(4):1715–1728, 2011.

[16] Hu Chen, Yi Zhang, Weihua Zhang, Peixi Liao, Ke Li, Jiliu Zhou, and Ge Wang. Low-dose ct denoising with convolutional neural network. In *2017 IEEE 14th International Symposium on Biomedical Imaging (ISBI 2017)*, pages 143–146. IEEE, 2017.

[17] Hu Chen, Yi Zhang, Mannudeep K Kalra, Feng Lin, Yang Chen, Peixi Liao, Jiliu Zhou, and Ge Wang. Low-dose ct with a residual encoder-decoder convolutional neural network. *IEEE transactions on medical imaging*, 36(12):2524–2535, 2017.

[18] Hu Chen, Yi Zhang, Yunjin Chen, Junfeng Zhang, Weihua Zhang, Huaiqiang Sun, Yang Lv, Peixi Liao, Jiliu Zhou, and Ge Wang. Learn: Learned experts' assessment-based reconstruction network for sparse-data ct. *IEEE transactions on medical imaging*, 37(6):1333–1347, 2018.

[19] Wenjun Xia, Zexin Lu, Yongqiang Huang, Yan Liu, Hu Chen, Jiliu Zhou, and Yi Zhang. Ct reconstruction with pdf: Parameter-dependent framework for data from multiple geometries and dose levels. *IEEE Transactions on Medical Imaging*, 2021.

[20] Wenjun Xia, Zexin Lu, Yongqiang Huang, Zuoqiang Shi, Yan Liu, Hu Chen, Yang Chen, Jiliu Zhou, and Yi Zhang. Magic: Manifold and graph integrative convolutional network for low-dose ct reconstruction. *IEEE Transactions on Medical Imaging*, 2021.

[21] Ian Goodfellow, Jean Pouget-Abadie, Mehdi Mirza, Bing Xu, David Warde-Farley, Sherjil Ozair, Aaron Courville, and Yoshua Bengio. Generative adversarial nets. *Advances in neural information processing systems*, 27, 2014.

[22] Justin Johnson, Alexandre Alahi, and Li Fei-Fei. Perceptual losses for real-time style transfer and super-resolution. In *European conference on computer vision*, pages 694–711. Springer, 2016.

[23] Jelmer M Wolterink, Tim Leiner, Max A Viergever, and Ivana Išgum. Generative adversarial networks for noise reduction in low-dose ct. *IEEE transactions on medical imaging*, 36(12):2536–2545, 2017.

[24] Mehdi Mirza and Simon Osindero. Conditional generative adversarial nets. *arXiv preprint arXiv:1411.1784*, 2014.

[25] Qingsong Yang, Pingkun Yan, Yanbo Zhang, Hengyong Yu, Yongyi Shi, Xuanqin Mou, Mannudeep K Kalra, Yi Zhang, Ling Sun, and Ge Wang. Low-dose ct image denoising using a generative adversarial network with wasserstein distance and perceptual loss. *IEEE transactions on medical imaging*, 37(6):1348–1357, 2018.

[26] Bent Fuglede and Flemming Topsoe. Jensen-shannon divergence and hilbert space embedding. In *International Symposium onInformation Theory, 2004. ISIT 2004. Proceedings.*, page 31. IEEE, 2004.

[27] Karen Simonyan and Andrew Zisserman. Very deep convolutional networks for large-scale image recognition. *arXiv preprint arXiv:1409.1556*, 2014.

[28] Jun-Yan Zhu, Taesung Park, Phillip Isola, and Alexei A Efros. Unpaired image-to-image translation using cycle-consistent adversarial networks. In *Proceedings of the IEEE international conference on computer vision*, pages 2223–2232, 2017.

[29] Xue Dong, Yang Lei, Sibo Tian, Tonghe Wang, Pretesh Patel, Walter J Curran, Ashesh B Jani, Tian Liu, and Xiaofeng Yang. Synthetic mri-aided multi-organ segmentation on male pelvic ct using cycle consistent deep attention network. *Radiotherapy and Oncology*, 141:192–199, 2019.

[30] Yingzi Liu, Yang Lei, Tonghe Wang, Yabo Fu, Xiangyang Tang, Walter J Curran, Tian Liu, Pretesh Patel, and Xiaofeng Yang. Cbct-based synthetic ct generation using deep-attention cyclegan for pancreatic adaptive radiotherapy. *Medical physics*, 47(6):2472–2483, 2020.

[31] Geoffrey Hinton, Oriol Vinyals, and Jeff Dean. Distilling the knowledge in a neural network. *arXiv preprint arXiv:1503.02531*, 2015.

[32] Seyed Iman Mirzadeh, Mehrdad Farajtabar, Ang Li, Nir Levine, Akihiro Matsukawa, and Hassan Ghasemzadeh. Improved knowledge distillation via teacher assistant. In *Proceedings of the AAAI Conference on Artificial Intelligence*, volume 34, pages 5191–5198, 2020.

[33] Adriana Romero, Nicolas Ballas, Samira Ebrahimi Kahou, Antoine Chassang, Carlo Gatta, and Yoshua Bengio. Fitnets: Hints for thin deep nets. *arXiv preprint arXiv:1412.6550*, 2014.

[34] Yulun Zhang, Kunpeng Li, Kai Li, Lichen Wang, Bineng Zhong, and Yun Fu. Image super-resolution using very deep residual channel attention networks. In *Proceedings of the European conference on computer vision (ECCV)*, pages 286–301, 2018.

[35] Jifeng Dai, Haozhi Qi, Yuwen Xiong, Yi Li, Guodong Zhang, Han Hu, and Yichen Wei. Deformable convolutional networks. In *Proceedings of the IEEE international conference on computer vision*, pages 764–773, 2017.

[36] Xizhou Zhu, Han Hu, Stephen Lin, and Jifeng Dai. Deformable convnets v2: More deformable, better results. In *Proceedings of the IEEE/CVF Conference on Computer Vision and Pattern Recognition*, pages 9308–9316, 2019.

[37] Saurabh Gupta, Judy Hoffman, and Jitendra Malik. Cross modal distillation for supervision transfer. In *Proceedings of the IEEE conference on computer vision and pattern recognition*, pages 2827–2836, 2016.

[38] Jong-Chyi Su and Subhransu Maji. Adapting models to signal degradation using distillation. *arXiv preprint arXiv:1604.00433*, 2016.

[39] Raia Hadsell, Sumit Chopra, and Yann LeCun. Dimensionality reduction by learning an invariant mapping. In *2006 IEEE Computer Society Conference on Computer Vision and Pattern Recognition (CVPR'06)*, volume 2, pages 1735–1742. IEEE, 2006.

[40] Olivier Henaff. Data-efficient image recognition with contrastive predictive coding. In *International Conference on Machine Learning*, pages 4182–4192. PMLR, 2020.

[41] Yonglong Tian, Dilip Krishnan, and Phillip Isola. Contrastive multiview coding. In *Computer Vision–ECCV 2020: 16th European Conference, Glasgow, UK, August 23–28, 2020, Proceedings, Part XI 16*, pages 776–794. Springer, 2020.

[42] Pierre Sermanet, Corey Lynch, Yevgen Chebotar, Jasmine Hsu, Eric Jang, Stefan Schaal, Sergey Levine, and Google Brain. Time-contrastive networks: Self-supervised learning from video. In *2018 IEEE international conference on robotics and automation (ICRA)*, pages 1134–1141. IEEE, 2018.

[43] Kaiming He, Haoqi Fan, Yuxin Wu, Saining Xie, and Ross Girshick. Momentum contrast for unsupervised visual representation learning. In *Proceedings of the IEEE/CVF Conference on Computer Vision and Pattern Recognition*, pages 9729–9738, 2020.

[44] Ting Chen, Simon Kornblith, Mohammad Norouzi, and Geoffrey Hinton. A simple framework for contrastive learning of visual representations. In *International conference on machine learning*, pages 1597–1607. PMLR, 2020.

[45] Olivier Henaff. Data-efficient image recognition with contrastive predictive coding. In *International Conference on Machine Learning*, pages 4182–4192. PMLR, 2020.

[46] Taesung Park, Alexei A Efros, Richard Zhang, and Jun-Yan Zhu. Contrastive learning for unpaired image-to-image translation. In *European Conference on Computer Vision*, pages 319–345. Springer, 2020.

[47] Haiyan Wu, Yanyun Qu, Shaohui Lin, Jian Zhou, Ruizhi Qiao, Zhizhong Zhang, Yuan Xie, and Lizhuang Ma. Contrastive learning for compact single image dehazing. In *Proceedings of the IEEE/CVF Conference on Computer Vision and Pattern Recognition (CVPR)*, pages 10551–10560, June 2021.

[48] Olaf Ronneberger, Philipp Fischer, and Thomas Brox. U-net: Convolutional networks for biomedical image segmentation. In *International Conference on Medical image computing and computer-assisted intervention*, pages 234–241. Springer, 2015.

[49] Vincent Dumoulin and Francesco Visin. A guide to convolution arithmetic for deep learning. *arXiv preprint arXiv:1603.07285*, 2016.

[50] Christian Szegedy, Sergey Ioffe, Vincent Vanhoucke, and Alexander A Alemi. Inception-v4, inception-resnet and the impact of residual connections on learning. In *Thirty-first AAAI conference on artificial intelligence*, 2017.

[51] Nikolay Kyurkchiev and Svetoslav Markov. Sigmoid functions: some approximation and modelling aspects. *LAP LAMBERT Academic Publishing, Saarbrucken*, 2015.

[52] Xiangyu Xu, Muchen Li, and Wenxiu Sun. Learning deformable kernels for image and video denoising. *arXiv preprint arXiv:1904.06903*, 2019.

[53] Alex Krizhevsky, Ilya Sutskever, and Geoffrey E Hinton. Imagenet classification with deep convolutional neural networks. *Advances in neural information processing systems*, 25:1097–1105, 2012.

[54] Ross Girshick. Fast r-cnn. In *Proceedings of the IEEE international conference on computer vision*, pages 1440–1448, 2015.

[55] Zhou Wang, Alan C Bovik, Hamid R Sheikh, and Eero P Simoncelli. Image quality assessment: from error visibility to structural similarity. *IEEE transactions on image processing*, 13(4):600–612, 2004.

[56] Allan Donner, Mohamed M Shoukri, Neil Klar, and Emma Bartfay. Testing the equality of two dependent kappa statistics. *Statistics in medicine*, 19(3):373–387, 2000.